

Prompt high-energy neutrinos from gamma-ray bursts in photospheric and synchrotron self-Compton scenarios

Kohta Murase

Yukawa Institute for Theoretical Physics, Kyoto University, Kyoto, 606-8502, Japan

(Dated: November 19, 2008)

We investigate neutrino emission from gamma-ray bursts (GRBs) under alternative scenarios for prompt emission (the photospheric and synchrotron self-Compton scenarios) rather than the classical optically thin synchrotron scenario. In the former scenario, we find that neutrinos from the pp reaction can be very important at energies $\lesssim (10 - 100)$ TeV. They may be detected by IceCube/KM3Net and useful as a probe of baryon acceleration around/below the photosphere. In the latter scenario, we may expect \sim EeV $p\gamma$ neutrinos produced by soft photons. Predicted spectra are different from that in the classical scenario, and neutrinos would be useful as one of the clues to the nature of GRBs (the jet composition, emission radius, magnetic field and so on).

PACS numbers: 98.70.Rz, 95.85.Ry

I. INTRODUCTION

Prompt high-energy neutrino emission from gamma-ray bursts (GRBs) was predicted in the internal shock (IS) model [1, 2] and has been studied by many authors [3, 4, 5] (for afterglows, see Ref. [6] and references therein). However, despite recent progresses in the *Swift* era, the mechanism of prompt emission has not been well understood [7]. One of the most frequently discussed scenarios as a standard one is the classical optically thin synchrotron (including diffusive synchrotron) scenario, where prompt photons around the peak energy in the hard x-ray or gamma-ray band come from electrons accelerated at internal shocks and/or by magnetic reconnection in the optically thin region. However, this scenario cannot satisfactorily explain some observational features such as the lower energy spectral index and observed spectral correlations [8], which may also be related to the cooling and efficiency problems [9]. Motivated by these problems, photospheric emission models have been developed [10, 11], which have an advantage to stabilize the peak energy [10, 12].

Another alternative scenario is the synchrotron self-Compton (SSC) scenario, which may provide more viable parameter sets for prompt emission, compared to the classical scenario [13]. The synchrotron peak is in the optical/ultraviolet range and gamma-ray photons arise from inverse Compton scatterings. This scenario may explain some bursts such as GRB 080319B [14], despite the lack of bright optical emission in many bursts [15].

In this work, we investigate neutrino emission under photospheric and SSC scenarios. Our method of calculation based on Geant4 is basically the same as in Refs. [3, 6], but improved qualitatively and quantitatively by including the pp reaction and all the relevant processes of protons, mesons and muons [16, 17]. As for GRB neutrinos, cooling of mesons and muons is remarkably important, which makes neutrino spectra complicated and affects estimate of event rates [2, 5, 17]. Especially, we demonstrate that pp neutrinos can be important below

 ~ 100 TeV.

II. THE PHOTOSPHERIC SCENARIO

GRB prompt emission is considered to be radiation from a highly relativistic jet toward us, and the typical Lorentz factor of the collimated outflow is $\Gamma \sim 10^{2-3}$. In the standard picture, a significant fraction of the outflow energy is converted to the radiation energy via some dissipation mechanism within the outflow (e.g., internal shocks or magnetic reconnection), leading to the observed isotropic photon luminosity $L_\gamma \sim 10^{52}$ ergs s^{-1} [7]. In photospheric emission models, the prompt emission comes from around the photospheric radius $r \sim r_{\text{ph}}$, at which the Thomson optical depth $\tau_{\gamma e} \simeq n_e \sigma_T (r/\Gamma)$ is unity. The photospheric radius is given by $r_{\text{ph}} \approx (L_M \sigma_T / 4\pi \Gamma^3 m_p c^3) \simeq 1.2 \times 10^{12}$ cm $L_{M,52.5} \Gamma_{2.5}^{-3}$, when the outflow is baryonic ($n_e \approx n_p$). Here L_M is the isotropic outflow luminosity carried by baryons, in the observer frame [7, 10]. Possibly, the outflow may be dominated by pairs. If $n_e/n_p \sim m_p/m_e$, we obtain $r_{\text{ph}} \approx (L_M \sigma_T / 4\pi \Gamma^3 m_e c^3) \simeq 2.2 \times 10^{15}$ cm $L_{M,52.5} \Gamma_{2.5}^{-3}$ [11]. In this scenario, dissipation and thermalization should occur around/below the photosphere. For instance, in the dissipative photospheric model [11], we can assume that the dissipation is maintained after the coasting radius, leading to the temperature $kT_{\text{ob}} \sim 100$ keV in the observer frame. The observed peak energy $\varepsilon_{\text{ob}}^b \sim 500$ keV can be achieved by the Comptonized thermal photons [12].

As an example, let us consider an internal collision of two subshells in the relativistic outflow, with $\Gamma_s \sim 10^2$ and $\Gamma_f \sim 10^3$. The Lorentz factor of the merged subshell is estimated as $\Gamma \approx \sqrt{\Gamma_f \Gamma_s} \simeq 10^{2.5}$, and the Lorentz factor of the internal shock in their center of mass frame is $\sim \sqrt{\Gamma_{\text{sh}}} \approx \sqrt{(\Gamma_f/\Gamma_s + \Gamma_s/\Gamma_f)/2} \sim$ a few. Hence, internal shocks would be mildly relativistic shocks, at which electrons can be accelerated, and prompt emission mainly comes from the shocked subshells which could

be magnetized via plasma instabilities at collisions [7]. Not only electrons but also baryons can be accelerated even around/below the photosphere [9, 17]. The acceleration time scale of protons in the comoving frame of the merged subshells is written as $t_{\text{acc}} = \eta \varepsilon_p / eBc$. Although realistic values of η are not well known, we could expect $\eta \sim (1 - 10)$ in the most efficient cases, when we consider the Fermi acceleration mechanism in the Bohm limit [5, 18]. Here we assume $\eta \sim 10$ as in Refs. [3, 5]. The magnetic field is written as $B \approx 8.4 \times 10^5 \text{ G } \xi_B^{1/2} L_{\gamma,52}^{1/2} \Gamma_{2.5}^{-1} r_{\text{ph},12.5}^{-1}$, where $\xi_B \equiv U_B / U_\gamma$. Although ξ_B is uncertain, we expect that the equipartition between the magnetic energy density U_B and photon energy density U_γ can be achieved in the photospheric scenario, as often expected in the classical one. The maximum energy of protons is set by the condition $t_{\text{acc}} < \min[t_p, t_{\text{dyn}}]$. Here $t_{\text{dyn}} \approx r/\Gamma c$ is the dynamical time scale and $t_p^{-1} \equiv t_{\text{BH}}^{-1} + t_{p\gamma}^{-1} + t_{pp}^{-1} + t_{\text{syn}}^{-1} + t_{\text{IC}}^{-1} + t_{\text{ad}}^{-1} + t_{\text{esc}}^{-1}$ is the proton loss time scale (in the comoving frame), where t_{BH} , $t_{p\gamma}$, t_{pp} , t_{syn} , t_{IC} , t_{ad} , and t_{esc} are cooling times of the Bethe-Heitler process, photomeson production, pp reaction, synchrotron emission, inverse Compton emission, adiabatic expansion, and the escape time in the Bohm diffusion approximation [5, 6]. Following Refs. [3, 6], we evaluate the maximum proton energy for each parameter set, whose typical values are $E_p^{\text{max}} \sim 10^{8-10}$ GeV, in the observer frame.

High-energy protons can interact with photons and protons, producing mesons and muons that decay to neutrinos. As in Refs. [2, 3, 4, 6], it is often convenient to use the effective photomeson production optical depth, $f_{p\gamma} \approx t_{\text{dyn}}/t_{p\gamma}$. By using the Δ -resonance approximation at $E_p^b \sim 50 \text{ PeV } \Gamma_{2.5}^2 / \varepsilon_{\text{ob},316 \text{ keV}}^b$ [2, 3, 4, 6], we have $f_{p\gamma}(E_p^b) \simeq 23 \frac{L_{\gamma,51.5}^b \Gamma_{2.5}}{L_{M,52.5} \varepsilon_{\text{ob},316 \text{ keV}}^b} \tau_{\gamma e}$, where $L_\gamma (< L_\gamma)$ is the observed photon luminosity at $\varepsilon_{\text{ob}}^b$. It implies that almost all the energy of high-energy protons can be used for photomeson production when $t_{p\gamma}$ is the most important, and accelerated protons will be depleted. Similarly, the effective optical depth for pp reaction is $f_{pp} \approx \kappa_{pp} n_p \sigma_{pp} l \simeq 0.05 \tau_{\gamma e}$, where $\sigma_{pp} \simeq 5 \times 10^{-26} \text{ cm}^{-2}$ and $\kappa_{pp} \simeq 0.5 - 0.6$. The meson production efficiency f_{meson} can be approximated by $\sim \min[1, \max(f_{p\gamma}, f_{pp})]$, as long as $t_{p\gamma}$ or t_{pp} is the most relevant loss time scale. We can expect that a significant fraction of proton energy is used for meson production, which is demonstrated through numerical calculations.

III. THE SSC SCENARIO

SSC emission models have often been discussed [13], where the observed peak energy $\varepsilon_{\text{ob}}^b \sim 500 \text{ keV}$ is identified with the second peak formed by up-scattered synchrotron photons. Rather large emission radii close to the deceleration radius, $r_{\text{dec}} \sim 10^{16} \text{ cm}$ ($\gg r_{\text{ph}} \sim 10^{12} \text{ cm}$) are expected [13, 14]. The first synchrotron peak in the observer frame is estimated as $\varepsilon_{\text{ob}}^{b1} \approx$

$\hbar \gamma_{e,m}^2 (\Gamma eB/m_e c) \sim 20 \text{ eV } \varepsilon_{e,-1}^2 \xi_{B,-2}^{1/2} L_{\gamma,52}^{1/2} r_{15.5}^{-1}$, and then the second peak coming from inverse Compton scatterings is $\varepsilon_{\text{ob}}^{b2} \approx \gamma_{e,m}^2 \varepsilon_{\text{ob}}^{b1} \sim 700 \text{ keV } \varepsilon_{e,-1}^4 \xi_{B,-2}^{1/2} L_{\gamma,52}^{1/2} r_{15.5}^{-1}$. In addition, the third peak of $\varepsilon_{\text{ob}}^{b3} \sim 20 \text{ GeV}$ can also be expected, which is one of the predictions in this scenario. Most of the radiation energy can be released as high-energy gamma rays, so that we expect $\mathcal{E}_\gamma^{\text{iso}} \simeq Y \mathcal{E}_\gamma^{\text{iso}}$ with $Y \sim \xi_B^{-1/2}$, where Y is the Compton Y parameter [7] and $\mathcal{E}_\gamma^{\text{iso}}$ is the isotropic energy around the second peak.

Note that, in this scenario, the magnetic field should be smaller than in the equipartition case. Corresponding to $Y \sim 10$, $\xi_B \equiv U_B / U_\gamma \sim 10^{-2}$ leads to $B \sim 46 \text{ G } \xi_{B,-2}^{1/2} L_{\gamma,52}^{1/2} \Gamma_{2.5}^{-1} r_{15.5}^{-1}$. Then, from the condition $t_{\text{acc}} < \min[t_p, t_{\text{dyn}}]$, the maximum proton energy is typically estimated as $E_p^{\text{max}} \sim 10^{10-11}$ GeV for $\eta \sim 10$. Production of ultra-high-energy cosmic rays (UHECRs) may be possible.

We can also evaluate the effective photomeson optical depth as $f_{p\gamma}(E_p) \simeq 9 \frac{L_{\gamma,50.5}^{b1}}{r_{15.5} \Gamma_{2.5}^2 \varepsilon_{\text{ob},32 \text{ eV}}^{b1}} (E_p / E_p^{b1})^{\beta-1}$, at sufficiently high energies below $E_p^{b1} \sim 500 \text{ EeV } \Gamma_{2.5}^2 / \varepsilon_{\text{ob},32 \text{ eV}}^{b1}$. When $t_{p\gamma}$ is the most relevant, we expect a significant fraction of proton energy is used for the photomeson production around the highest energies. But, in this scenario, $f_{p\gamma}$ and f_{pp} are rather small at lower energies, so that efficient $\lesssim \text{PeV}$ neutrino production is not expected.

IV. THE NEUTRINO SPECTRUM AND FLUX

In this work, we numerically calculate neutrino spectra and evaluate fluxes through the method used in Refs. [3, 6]. Calculations are first executed in the comoving frame, and then results in the observer frame can be easily obtained via the transformation. The photomeson production and pp reaction are treated in detail, as well as various cooling processes of mesons and muons, i.e., synchrotron, inverse Compton, meson-photon, $\pi p / \mu p$ and adiabatic cooling processes. Neutrino spectra can be calculated, giving a target photon spectrum with $U_\gamma = (L_\gamma / 4\pi r^2 \Gamma^2 c)$, target (thermal) proton density $n_p = (U_{\text{th}} / m_p c^2)$ and $U_B = \xi_B U_\gamma$. For the evaluation of neutrino fluxes, proton fluxes should also be given and we use $dn_{\text{CR}}/d\varepsilon_p \propto \varepsilon_p^{-2}$ in this work. Although the proton spectral index of $p \sim 2$ is often expected for nonrelativistic or mildly relativistic shocks with the compression ratio of ~ 4 , different values are possible, for example, due to large angle scatterings rather than small pitch-angle scatterings across relativistic shocks [18, 19]. The baryon energy input \mathcal{E}_{CR} is given by using the nonthermal baryon loading factor $\xi_{\text{acc}} \equiv \mathcal{E}_{\text{CR}} / \mathcal{E}_\gamma = \mathcal{E}_{\text{CR}}^{\text{iso}} / \mathcal{E}_\gamma^{\text{iso}}$, where \mathcal{E}_γ and $\mathcal{E}_\gamma^{\text{iso}}$ are the geometrically corrected radiation energy and isotropic radiation energy, respectively. Here we adopt $\xi_{\text{acc}} \sim 1 - 10$, as in Refs. [2, 3, 4, 6]. Differences in spectra mainly come from r , ξ_B and the photon spectrum, which depend on prompt emission scenarios.

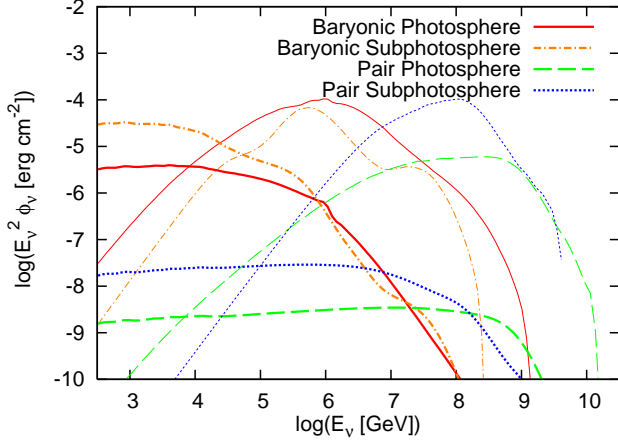


FIG. 1: The $(\nu_\mu + \bar{\nu}_\mu)$ fluence from a GRB event at $z = 0.1$. pp neutrinos (thick line) and $p\gamma$ neutrinos (thin line) are shown. Baryonic photosphere: $r = r_{\text{ph}} = 10^{12.5}$ cm ($\tau_{\gamma e} = 1$); $N_\mu \sim 1.7$ events. Baryonic subphotosphere: $r = 10^{-0.5} r_{\text{ph}}$ ($\tau_{\gamma e} = 10$); $N_\mu \sim 1.4$ events. Pair photosphere: $r = r_{\text{ph}} = 10^{14.2}$ cm ($\tau_{\gamma e} = 1$); $N_\mu \sim 0.018$ events. Pair subphotosphere: $r = 10^{-0.5} r_{\text{ph}}$ ($\tau_{\gamma e} = 10$); $N_\mu \sim 0.16$ events. $\mathcal{E}_\gamma^{\text{iso}} = 10^{53.5}$ ergs, $\Gamma = 10^{2.5}$, $\xi_B = 1$, and $\xi_{\text{acc}} = 1$ are adopted. We assume $n_e = n_p$ in case of the baryonic photosphere while $n_e = \frac{m_p}{m_e} n_p$ in possible cases of the pair photosphere.

For instance, in the classical scenario, $r \sim 10^{13-15}$ cm, $\xi_B \sim 1$ and the broken power-law photon spectrum are typically used [2, 3, 4, 5].

In the photospheric scenario, we may expect smaller radii of $r \sim 10^{11-13}$ cm and strong magnetic fields with $\xi_B \sim 1$. Prompt emission comes from the photosphere where $\tau_{\gamma e} = 1$, so that we can adopt the broken power-law photon spectrum as $dn/d\varepsilon \propto (\varepsilon/\varepsilon^b)^{-\alpha}$ for $\varepsilon^{\text{min}} < \varepsilon < \varepsilon^b$ and $dn/d\varepsilon \propto (\varepsilon/\varepsilon^b)^{-\beta}$ for $\varepsilon^b < \varepsilon < \varepsilon^{\text{max}}$, expressed in the comoving frame. Here we set $\varepsilon^{\text{min}} = 1$ eV and $\varepsilon^{\text{max}} = 1$ MeV, because the synchrotron self-absorption and pair-creation absorption will be crucial below and above these energies, respectively. But our results are not sensitive to them. We take $\varepsilon^b = \varepsilon_{\text{ob}}^b/\Gamma = 1$ keV, $\alpha = 1$ and $\beta = 2.2$, which are obtained from observations. However, since photons would be significantly thermalized when $\tau_{\gamma e} > 1$, we adopt the black-body photon spectrum with the temperature $T = (U_\gamma/a)^{1/4}$ for subphotospheric emission. n_p is given assuming $U_{\text{th}} = U_\gamma$, and we use $\tau_{\gamma e}$ as a parameter instead of L_γ^b .

In the SSC scenario, we expect larger radii of $r \sim 10^{15-16}$ cm and relatively weak magnetic fields with $\xi_B \sim 0.01$. The photon spectrum is given by the sum of multi-broken power-law spectra with break energies, $\varepsilon^{b1} = (10^{-2} - 10^{-1})$ eV and $\varepsilon^{b2} = 1$ keV with $\alpha = 1$ and $\beta = 2.2$. Note that larger emission radii lead to lower synchrotron self-absorption energies of $\varepsilon^{\text{min}} = (10^{-3} - 10^{-1})$ eV. For comparison, we also show neutrinos produced via the $p\gamma$ reaction between protons accelerated at the external reverse-shock (RS) and prompt photons produced

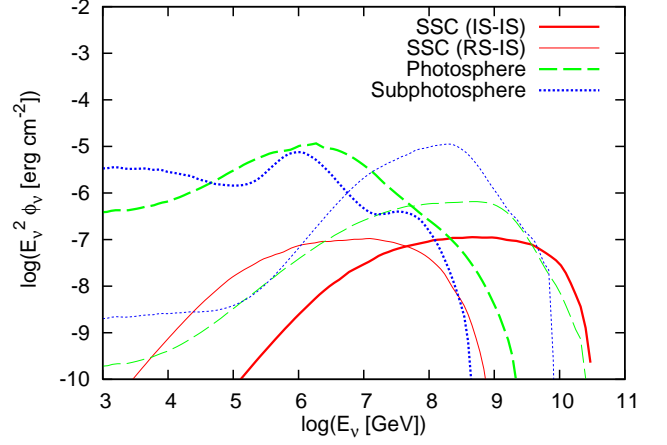


FIG. 2: As in Fig. 1, but $z = 0.9$. SSC (IS-IS) (thick solid line): $r = 10^{16}$ cm, $\Gamma = 10^3$, $L_\gamma^b = 10^{52.3}$ ergs s $^{-1}$, and $\xi_B = 0.01$; $N_\mu \sim 2 \times 10^{-4}$ events. SSC (RS-IS) (thin solid line): $r_\times \simeq 10^{16.4}$ cm, $\Gamma_\times \simeq 150$, and $B_\times^r \simeq 7.7$ G (coming from $E_{\text{ej}}^{\text{iso}} = 4 \times 10^{54}$ ergs, $\Delta_0 = 7.5 \times 10^{11}$ cm, $\epsilon_B^r/f_B^r = 4 \times 10^{-3}$, and $A_* = 0.4$, inferred in Refs. [14]); $N_\mu \sim 10^{-3}$ events. For SSC, $\mathcal{E}_{\gamma 2}^{\text{iso}} = 10^{54.5}$ ergs, $\alpha = 0.86$, $\beta = 3.6$, and $\xi_{\text{acc}} = 1$. Photosphere (baryonic) (thick dashed line): $r = r_{\text{ph}} = 10^{12.5}$ cm; $N_\mu \sim 0.2$ events. Photosphere (pair) (thin dashed line): $r = r_{\text{ph}} = 10^{14.2}$ cm; $N_\mu \sim 2 \times 10^{-3}$ events. Subphotosphere (baryonic) (thick dotted line): $r = 10^{-0.5} r_{\text{ph}}$; $N_\mu \sim 0.2$ events. Subphotosphere (pair) (thin dotted line): $r = 10^{-0.5} r_{\text{ph}}$; $N_\mu \sim 10^{-2}$ events. For photosphere and subphotosphere, $\mathcal{E}_\gamma^{\text{iso}} = 10^{54.5}$ ergs, $\xi_B = 1$, and $\xi_{\text{acc}} = 1$.

by internal dissipation. The relevant quantities at the crossing time, such as the radius r_\times , Lorentz factor of the shocked ejecta Γ_\times and magnetic field B_\times , are evaluated according to the standard reverse-forward shock theory [7]. The procedure is described in Ref. [6].

The results in the photospheric scenario are shown in Fig. 1. We can see a pp neutrino component is dominant at $E_\nu \lesssim 10$ TeV, and more important for subphotospheric emission. The Bethe-Heitler and photomeson production processes become more relevant at higher energies. The former can lead to a dip between pp and $p\gamma$ components (dotted-dashed lines). The latter makes $p\gamma$ neutrinos, whose fluence is suppressed at sufficiently high energies since mesons and muons cool before they decay. For example, we can find break energies around PeV, and $p\gamma$ neutrinos from kaons at higher energies $E_\nu \gtrsim 10$ PeV, for baryonic photosphere and baryonic subphotosphere. When the subphotospheric emission is expected, dissipation would continue from the subphotospheres all the way to the photosphere, enabling us to expect that pp neutrinos from subphotospheres are more important at lower energies, while $p\gamma$ neutrinos from around/above the photosphere at higher energies. Muon event rates expected by IceCube, $N_\mu(> 10^{2.5} \text{ GeV})$, are also shown in the figure caption. If a burst occurs at $z \lesssim 0.1$, we may detect a few events. Event rates of pp neutrinos dominate over those of $p\gamma$ neutrinos for baryonic subphotosphere.

In Fig. 2, we show neutrino spectra in the SSC and photospheric scenarios for an energetic burst such as GRB 080319B. In the SSC scenario, expected event rates are few due to the small photon density at large radii. Note that neutrinos coming from protons accelerated at the reverse shock are dominant at lower energies [see SSC (RS-IS)]. It is because reverse-shock protons interact with blue-shifted prompt photons, which are assumed to have the steep photon spectrum with $\beta = 3.6$ (solid lines) [14]. In the photospheric scenario, we can expect higher neutrino fluences than in the other scenarios.

It is important to consider the cumulative neutrino background, since the time- and space-coincidence is expected for GRB neutrino emission [4]. The background flux can be roughly estimated as [2, 3, 4]

$$E_\nu^2 \Phi_\nu \sim 3 \times 10^{-9} \text{GeV cm}^{-2} \text{s}^{-1} \text{str}^{-1} \tilde{\mathcal{E}}_{\text{HECR},51} \times \frac{f_{\text{mes}}(E_\nu)}{0.5} \frac{f_{\text{sup}}(E_\nu)}{0.5} \frac{f_z}{3} \frac{R_{\text{GRB}}(0)}{20 \text{Gpc}^{-3} \text{yr}^{-1}}, \quad (1)$$

where f_{sup} is the suppression factor due to cooling of mesons and muons [2, 5, 6, 17] and f_z expresses the contribution from the high redshift GRBs [2, 3]. Here $R_{\text{GRB}}(0)$ is the overall (not apparent) local rate, where GRBs are regarded as jets with $\mathcal{E}_\gamma \sim 10^{51}$ ergs [3, 7].

The results are shown in Fig. 3, where the GRB rate evolution is properly considered [6]. Predictions in the photospheric and SSC scenarios are rather different from the classical one. In the photospheric scenario, we expect larger event rates than others with the same baryon loading, and pp neutrinos may become important at $\lesssim (10 - 100)$ TeV. In the SSC scenario, we could expect $\sim (1 - 10)$ EeV neutrinos from interactions between UHECRs and soft photons, but note that our evaluation would be applied to only a fraction of GRBs [15].

V. IMPLICATIONS AND DISCUSSIONS

In the near future, high-energy neutrino signals may be detected by IceCube and KM3Net [20]. IceCube Deep Core for \sim TeV neutrinos and acoustic/radio and shower detectors for \sim EeV neutrinos will also be useful. In this work, we have first demonstrated that pp neutrinos can become more important than $p\gamma$ neutrinos in prompt neutrino emission, if the photospheric scenario is realized. Detection of $\lesssim (10 - 100)$ TeV neutrinos is important as a probe of dissipation and baryon acceleration around/below the photosphere as well as a diagnosis of the jet composition, although the detectability depends on the pair loading. Also, these photospheric neutrinos can be distinguished from precursor ones [17] through correlations of neutrinos with prompt photons. At higher energies, $p\gamma$ neutrinos become more important, and there may be contributions from optically thin internal shocks occurring above the photosphere. However, $p\gamma$ neutrinos cannot be expected for too large values of η , although we have assumed $\eta \sim 10$ so far. When $\eta \gtrsim 10^{3-4}$, only pp

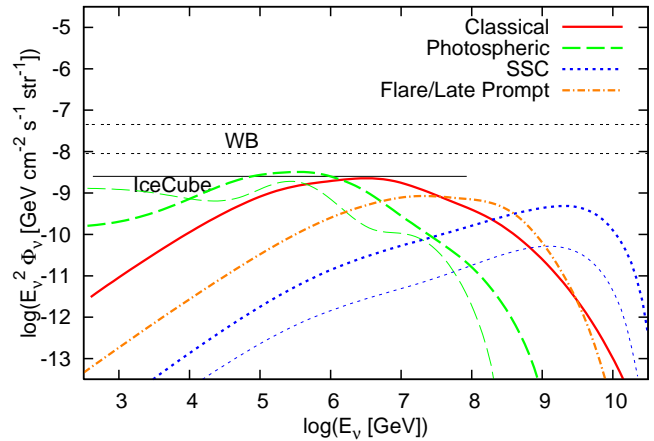


FIG. 3: The cumulative neutrino backgrounds from GRBs. Classical: originally predicted by Waxman and Bahcall [2] and the numerically calculated spectrum is taken from Refs. [3, 6], but averaged over sets A and B, $\Gamma = 10^{2.5}$ and $\xi_B = 1$; $N_\mu \sim 9.4$ events/yr. Photospheric (baryonic) (thick dashed line): $r = r_{\text{ph}} = 10^{12.5}$ cm, $\Gamma = 10^{2.5}$, and $\xi_B = 1$; $N_\mu \sim 24$ events/yr. Photospheric (baryonic) (thin dashed line): $r = 10^{-0.5} r_{\text{ph}}$, $\Gamma = 10^{2.5}$, and $\xi_B = 1$; $N_\mu \sim 16$ events/yr. SSC (IS-IS) (thick dotted line): $r = 10^{15.5}$ cm, $\Gamma = 10^{2.5}$, $L_\gamma^b = 10^{51.3}$ ergs s^{-1} , and $\xi_B = 0.01$; $N_\mu \sim 0.14$ events/yr. SSC (RS-IS) (thin dotted line): $r_\times \simeq 10^{16.9}$ cm, $\Gamma_\times \simeq 160$, and $B_\times^r \simeq 5.9$ G; $N_\mu \sim 0.014$ events/yr. Flare/late prompt: proposed by Murase and Nagataki [3] and the numerically calculated spectrum is taken from Refs. [3, 6] (the model LP0); $N_\mu \sim 1.2$ events/yr. WB: Waxman-Bahcall bounds shown as benchmarks [2]. The cosmic-ray proton energy input per logarithmic interval $\tilde{\mathcal{E}}_{\text{HECR}} \equiv \mathcal{E}_{\text{CR}}/R$ is normalized to 10^{51} ergs for the prompt emission scenarios while 10^{50} ergs for flare/late prompt. As a GRB rate evolution model, the GRB3 model in Ref. [6] is adopted with the cosmological parameters ($\Omega_m = 0.3, \Omega_\Lambda = 0.7; H_0 = 71 \text{ km s}^{-1} \text{ Mpc}^{-1}$) and $z_{\text{max}} = 11$.

neutrinos may be relevant. Note that our predicted fluxes are below the current AMANDA limit and Waxman-Bahcall bounds [21]. If neutrinos are not detected in the future, it implies that baryon acceleration is insufficient (small ξ_{acc} and/or very large η) or that prompt emission occurs sufficiently above the photosphere. In addition, we have demonstrated that synchrotron photons in the optical/ultraviolet range may enhance \sim EeV neutrinos in the SSC scenario, compared to the other scenarios. Cooling of meson and muons is not so important, and \sim EeV neutrinos will be useful as a probe of UHECR acceleration. Detection of them will also imply the nature of GRBs, e.g., r and ξ_B .

One may expect hadronic high-energy gamma rays can be detected by the recently launched *Fermi* satellite. For photospheric emission, we do not expect that high-energy gamma rays with $\varepsilon_{\text{ob}} \gtrsim$ a few $\times \Gamma m_e c^2$ escape from the source due to the large optical depth for pair creation [22]. Primary hadronic gamma rays induce the cascade in the source, and resulting spectra would be similar to

those in the classical scenario. However, as indicated in Asano and Inoue [23], it is not easy to find observational signatures of hadronic gamma rays with $\xi_B \sim 1$, $\xi_{\text{acc}} \sim 1$, $\alpha = 1$ and $\beta = 2.2$, considered by us. (Note that the steeper electron spectral index of $p_e \sim 3.0$ and softer low-energy photon index of $\alpha \sim 1.5$ in their calculations could lead to overestimating hadronic signatures in spectra [24].) Furthermore, we would not expect to distinguish between the classical and photospheric scenarios from signatures of cascaded hadronic gamma rays themselves. Hence, detection of $\lesssim (10 - 100)$ TeV pp neutrinos is more important as a unique probe. On the other hand, in the SSC scenario, primary high-energy gamma rays produced via the photomeson production could escape from the source. Their typical energy is \gtrsim EeV, and they cannot avoid attenuation by the cosmic background photons. The detectability of cascaded gamma rays in the GeV-TeV range strongly depends on the intergalactic magnetic field strength. Only when the intergalactic magnetic field is very weak, $B_{\text{IG}} \lesssim 10^{-16}$ G, we may detect them as a pair echo [25]. However, even in such cases, we expect that the pair echo emission would be subdominant compared to the primary leptonic emission. In fact, in the SSC scenario, strong high-energy

gamma rays should be generated through the SSC emission, and the isotropic radiation energy around the third peak, $\mathcal{E}_{\gamma 3}^{\text{iso}} \sim 10^{54.5}$ ergs, is larger than the isotropic energy of primary hadronic very high-energy gamma rays, $\mathcal{E}_{\gamma, \text{VHE}}^{\text{iso}} \sim 10^{53.5}$ ergs. Hence, it would be difficult to use hadronic gamma rays as a probe of baryon acceleration in the SSC scenario.

GRBs may be the origin of observed UHECRs, as is discussed in many papers. Note that, if the photospheric scenario is real, UHECR explanation is impossible due to strong proton losses at the highest energies. In the SSC scenario, UHECRs may be explained.

Acknowledgments

As this work was being completed, we became aware during the Nanjing GRB conference that Wang and Dai also studied subphotospheric emission independently, albeit with a simpler analytic formulation [26]. K. M. thanks X. Y. Wang, P. Mészáros, K. Asano and Y. Z. Fan. K. M. is supported by a Grant-in-Aid for JSPS.

-
- [1] B. Paczynski and G. Xu, *Astrophys. J.* **427**, 708 (1994).
 - [2] E. Waxman and J. Bahcall, *Phys. Rev. Lett.* **78**, 2292 (1997); *Phys. Rev. D* **59**, 023002 (1998).
 - [3] K. Murase and S. Nagataki, *Phys. Rev. D* **73**, 063002 (2006); *Phys. Rev. Lett.* **97**, 051101 (2006).
 - [4] C.D. Dermer and A. Atoyan, *Phys. Rev. Lett.* **91**, 071102 (2003); D. Guetta, D.W. Hooper, J. Alvarez-Muñiz, F. Halzen, and E. Reuveni, *Astropart. Phys.* **20**, 429 (2004); K. Asano, *Astrophys. J.* **623**, 967 (2005); J. Becker, M. Stamatikos, F. Halzen, and W. Rhode, *Astropart. Phys.* **25**, 118 (2006).
 - [5] J.P. Rachen and P. Mészáros, *Phys. Rev. D* **58**, 123005 (1998); J.P. Rachen, R.J. Protheroe, and K. Mannheim, *Nucl. Phys. B, Proc. Suppl.* **80**, 240 (2000); Mücke *et al.*, *Astropart. Phys.* **18**, 593 (2003); C.D. Dermer, *Astrophys. J.* **664**, 384 (2007).
 - [6] K. Murase, *Phys. Rev. D* **76**, 123001 (2007).
 - [7] P. Mészáros, *Rep. Prog. Phys.* **69**, 2259 (2006); B. Zhang, *Chin. J. Astron. Astrophys.* **7**, 1 (2007).
 - [8] R. Preece *et al.*, *Astrophys. J. Suppl. Ser.* **126**, 19 (2000); L. Amati, *Mon. Not. R. Astron. Soc.* **372**, 233 (2006).
 - [9] K. Ioka *et al.*, *Astrophys. J.* **670**, L77 (2007).
 - [10] P. Mészáros and M. Rees, *Astrophys. J.* **530**, 292 (2000); C. Thompson, P. Mészáros, and M.J. Rees, *Astrophys. J.* **666**, 1012 (2007).
 - [11] M.J. Rees and P. Mészáros, *Astrophys. J.* **628**, 847 (2005).
 - [12] A. Pe'er, P. Mészáros, and M.J. Rees, *Astrophys. J.* **642**, 995 (2006).
 - [13] A. Panaitescu and P. Mészáros, *Astrophys. J.* **544**, L17 (2000); P. Kumar and E. McMahon, *Mon. Not. R. Astron. Soc.* **384**, 33 (2008).
 - [14] P. Kumar and A. Panaitescu, arXiv:0805.0144; J.L. Racusin *et al.*, *Nature (London)* **455**, 183 (2008).
 - [15] P.W.A. Roming *et al.*, *Astrophys. J.* **652**, 1416 (2006).
 - [16] M.J. Chodorowski, A.A. Zdziarski, S.R. Sikora, *Astrophys. J.* **400**, 181 (1992); K. Murase, S. Inoue, and S. Nagataki, arXiv:0805.0104.
 - [17] P. Mészáros and E. Waxman, *Phys. Rev. Lett.* **87**, 171102 (2001); S. Razzaque, P. Mészáros, and E. Waxman, *Phys. Rev. D* **68**, 083001 (2003).
 - [18] J. Bednarz and M. Ostrowski, *Mon. Not. R. Astron. Soc.* **283**, 447 (1996); Y.A. Gallant and A. Achterberg, *Mon. Not. R. Astron. Soc.* **305**, L6 (1999); M. Ostrowski, arXiv:0801.1339.
 - [19] J. Kirk *et al.*, *Astrophys. J.* **542**, 235 (2000); U. Keshet and E. Waxman, *Phys. Rev. Lett.* **94**, 111102 (2005); J. Aoi, K. Murase, and S. Nagataki, *Mon. Not. R. Astron. Soc.* **383**, 1431 (2008).
 - [20] J. Ahrens *et al.*, *Astropart. Phys.* **20**, 507 (2004); U.F. Katz, *Nucl. Instrum. Methods Phys. Res., Sect. A* **567**, 457 (2006).
 - [21] A. Achterberg *et al.*, *Astrophys. J.* **674**, 357 (2008).
 - [22] Y. Lithwick and R. Sari, *Astrophys. J.* **555**, 540 (2001); K. Murase and K. Ioka, *Astrophys. J.* **676**, 1123 (2008).
 - [23] K. Asano and S. Inoue, *Astrophys. J.* **671**, 645 (2007).
 - [24] K. Murase, K. Ioka, S. Nagataki, and T. Nakamura, *Phys. Rev. D* **78**, 023005 (2008).
 - [25] K. Murase, K. Asano, and S. Nagataki, *Astrophys. J.* **671**, 1886 (2007).
 - [26] X.Y. Wang and D.G. Dai, arXiv:0807.0290.